JGR Space Physics

RESEARCH ARTICLE
10.1029/2019JA027075

Saturn's Plasmapause: Signature of Magnetospheric Dynamics

M.F. Thomsen[1] and **A.J. Coates**[2]

[1]Planetary Science Institute, Tucson, AZ, USA, [2]Mullard Space Science Laboratory, University College London, Dorking, UK

Key Points:
- Plasmapause separates flux tubes of dense cold plasma from those that have undergone tail reconnection, leaving a tenuous, heated population
- Plasmapause is identified as transition from mostly-dense-with-some-tenuous to mostly-tenuous-with-some-dense plasma electron populations
- Boundary is typically found near and slightly beyond 10 Rs from the planet and is closer to the planet on the night side than on the dayside

Supporting Information:
- Supporting Information S1

Correspondence to:
M. F. Thomsen,
mthomsen@psi.edu

Citation:
Thomsen, M. F., & Coates, A. J. (2019). Saturn's plasmapause: Signature of magnetospheric dynamics. *Journal of Geophysical Research: Space Physics*, *124*, 8804–8813. https://doi.org/10.1029/2019JA027075

Received 26 JUN 2019
Accepted 25 SEP 2019
Accepted article online 10 OCT 2019
Published online 19 NOV 2019

Abstract We explore the paradigm that Saturn's plasmapause marks the boundary between the magnetic flux tubes that have been circulating around the planet for some time, accumulating a dense load of Enceladus-sourced material, and those that have recently undergone tail reconnection, shedding the bulk of the cold plasma and retaining a more tenuous, heated population. A centrifugally driven interchange instability should develop at this boundary, producing fingers of outward propagating dense plasma and of inward propagating hot, tenuous plasma. The plasmapause should thus be identifiable as a transition from mostly-dense-with-some-tenuous to mostly-tenuous-with-some-dense plasma populations. Electron densities from the Cassini Plasma Spectrometer/Electron Spectrometer (CAPS/ELS) instrument are used to identify the location of this transition for all of the low-latitude (<5° from the magnetic equator) passes through Saturn's inner/middle magnetosphere. The boundary is typically found near and somewhat beyond L=10 (i.e., at ~10 Rs from the planet), with a local time asymmetry such that it is closer to the planet on the night side than on the day side.

Plain Language Summary In Saturn's inner magnetosphere, cold dense plasma originating from the moon Enceladus is transported outward into the outer magnetosphere, where Saturn's rapid rotation causes the magnetic field to become strongly distended and to pinch off in the nightside tail region, releasing cold plasma downtail, and returning hot, tenuous plasma on shortened, more-dipolar magnetic field lines back toward the inner magnetosphere. The boundary separating the returning tenuous plasma from the dense cold plasma that has not yet pinched off is the plasmapause. An interchange instability forms at this boundary, producing fingers of outward-propagating dense plasma and of inward-propagating hot, tenuous plasma. The plasmapause should thus be identifiable as a transition from mostly-dense-with-some-tenuous to mostly-tenuous-with-some-dense plasma populations. Electron densities from the Cassini Plasma Spectrometer/Electron Spectrometer (CAPS/ELS) instrument are used to identify the location of this transition for all of the low-latitude (<5° from the magnetic equator) passes through Saturn's inner/middle magnetosphere. The boundary is typically found near and somewhat beyond ~10 Rs from the planet, and it is closer to the planet on the night side than on the day side.

1. Introduction

Saturn's magnetosphere is often termed “internally driven” because the structure and dynamics are largely determined by a dominant plasma source that lies deep inside the magnetosphere (the water plumes of the moon Enceladus) and by processes driven by the planet's rapid rotation: (1) centrifugally-driven flux-tube interchange that delivers inner magnetospheric plasma to the middle magnetosphere and (2) magnetic reconnection of stretched, plasma-laden flux tubes, with ultimate down-tail loss of plasmoids containing Enceladus-sourced material (e.g., Thomsen, 2013, and references therein). Following the expulsion of a plasmoid, the planetward portion of a reconnected flux tube snaps back toward Saturn, carrying only a hot, tenuous plasma population that remains after the bulk of the cooler, denser material has been ejected in the plasmoid.

Thus, a boundary is formed in this region, separating recently-reconnected flux tubes populated by hot, tenuous plasma, from flux tubes that have not yet reconnected and are still loaded with cool, inner magnetospheric plasma. This boundary has been termed the “plasmapause” by Young et al. (2005), in analogy to the terrestrial transition between the cool, dense plasmasphere and the hot plasma sheet.

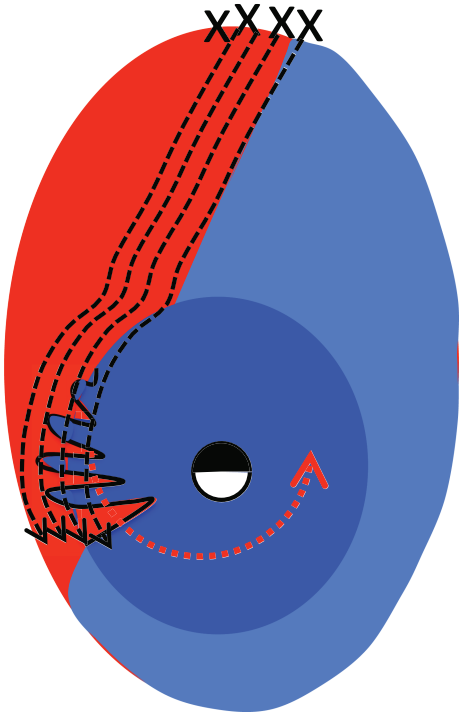

Figure 1. Illustration of loss of cold dense inner magnetospheric plasma (blue) from tail reconnection region (X), with subsequent dipolarization of heated, tenuous plasma that remains on the planetward-convecting, reconnected flux tubes (red). The black dashed arrows show the convective paths of the reconnected flux tubes. The boundary between the flux tubes that have undergone reconnection and those that have not (red/blue) is the plasmapause, and it is unstable to a centrifugally-driven interchange instability, producing alternating fingers of outward flowing dense plasma and inward flowing tenuous plasma. The red dashed arrow shows the inward penetration of the hot plasma under the influence of interchange.

The plasmapause at Saturn has been discussed more extensively by Thomsen et al. (2015), who presented Cassini observations that illustrated its formation.

The plasmapause boundary at Saturn represents a strong inward density gradient, which, because of Saturn's rapid rotation, is unstable to the centrifugally-driven interchange instability (e.g., Southwood & Kivelson, 1987). As a result, alternating fingers of hot, tenuous, inward-moving plasma and cool, dense, outward-moving plasma begin forming there. Figure 1 illustrates the sequence, from tail reconnection and hot-plasma injection to the growth of the instability and interpenetration of dense and tenuous fingers of plasma. Such fingers, both dense and tenuous, were observed in the event described by Thomsen et al. (2015). (We use the term "fingers," although it is also possible that the interchange produces more isolated flux tubes or "blobs." There is some evidence that the latter may be the case (Lai et al., 2016), but the matter is still under investigation.)

As a consequence of the interchange, the original density boundary of the plasmasphere becomes a more diffuse transition, roughly separating an interior region of dominantly cool, dense plasma (with frequent fingers of hot, tenuous, inflowing material) from an outer region of mostly hot, tenuous plasma (with outflowing fingers of dense material). The purpose of this paper is to identify, on an orbit-by-orbit basis, where this transition occurs. We will examine the temporal and LT variation of the location of the plasmapause, thus providing a global survey of the signature of tail reconnection.

2. Data and Analysis

The primary data used in this study are electron measurements obtained by the CAPS/ELS instrument (Cassini Plasma Spectrometer/Electron Spectrometer), specifically the electron density and temperature calculated by numerical integration of the observed counts (Lewis et al., 2008) and now available at the PDS. ELS is a top-hat electrostatic analyzer with eight separate anodes with different look directions in the viewing plane. Azimuthal coverage is provided by a physical actuator, which sweeps the viewing plane back and forth, resulting in coverage of ~2π sr of the sky. ELS covers an energy range of ~0.6 eV–28 keV (Coates et al., 1996; Linder et al., 1998; Young et al., 2004). The ELS moments available at PDS use measurements from Anode 5 only, assuming an isotropic distribution (Lewis et al., 2008). The temporal resolution of the derived moments is 32 s.

As noted above, the ELS moments are derived using only Anode 5 measurements, under the assumption that the electron distribution is isotropic. In fact, the electron distribution in Saturn's magnetosphere is often not isotropic. Depending on the orientation of the spacecraft, which varies rather frequently to accommodate various scientific objectives, this can result in an oscillation of the Anode-5-derived density as the actuator sweeps the field of view of Anode 5 back and forth across the peak of the distribution. This oscillation occurs at the actuation period (~7 min). Also, under some conditions, the spacecraft orientation may preclude Anode 5 from seeing the peak, even via actuation. Thus, there is some quantitative ambiguity regarding the derived densities, but the analysis procedure we describe below is rather insensitive to these oscillations.

For our analysis, we have merged the ELS moments with the spacecraft ephemeris using the CAPS ancillary (ANC) files also located in the PDS. We have discarded those few days for which one or more 6-hr ANC files were missing from the archive.

An example of the plasmapause transition described above is shown in Figure 2a (see Figure 1 of Thomsen et al., 2015, for another example). The figure shows the color-coded count rate (proportional to energy flux) from the CAPS/ELS instrument for 18 hours on 26–27 April 2010, while Cassini was inbound through the

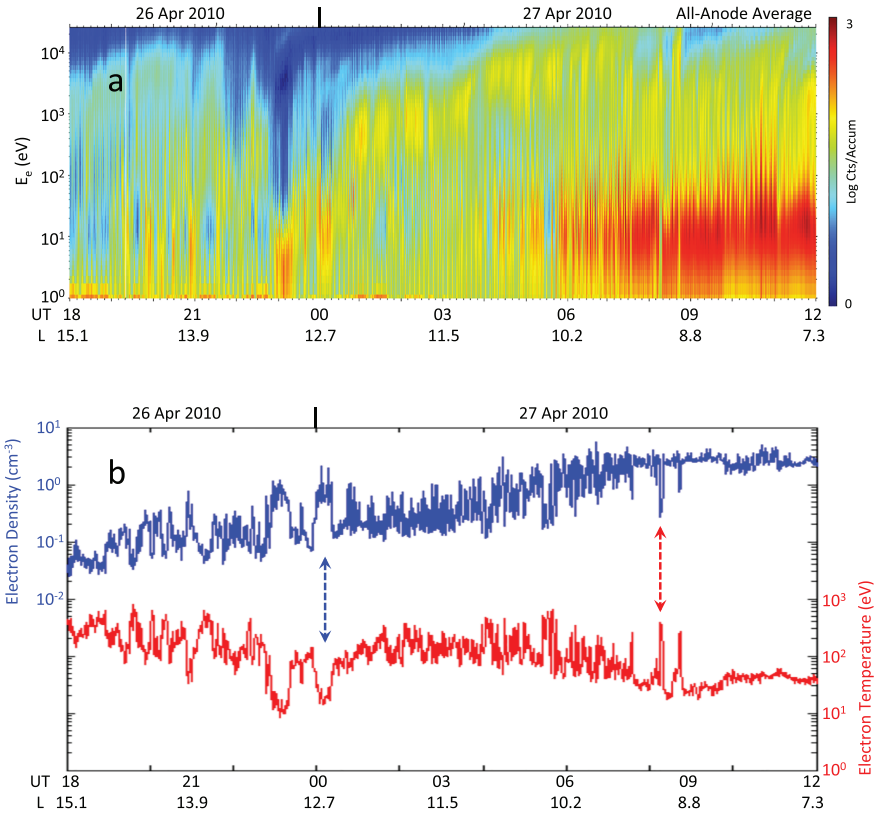

Figure 2. (a) Count rate of Cassini Plasma Spectrometer/Electron Spectrometer (CAPS/ELS) (proportional to energy flux) as a function of electron energy and time for an 18-hour interval on 26–27 April 2010, during which Cassini was inbound through the middle/inner magnetosphere at a latitude ~0° and a local time ~23 LT. (b) Corresponding electron density and temperature derived from measurements of ELS anode 5 (Lewis et al., 2008). Beyond L~10, the observations show alternating intervals of cold, dense material and hotter, more tenuous material. The blue vertical arrow highlights a cold, dense interval in the middle magnetosphere, and the red vertical arrow highlights a hot, tenuous interval in the inner magnetosphere (interchange injection).

night-side magnetosphere (LT~22–24) at a magnetic latitude of ~0°. Two principal populations are evident in the figure: A dense, cool population below ~100 eV and a more tenuous, hotter population above 100 eV. After ~1000 UT (i.e., inside of L~10.2) on 27 April, the cool dense population dominates, with occasional brief intervals of the hotter electrons. Prior to that time, the hotter population is seen most often, with occasional intervals of cooler material. Within the paradigm described above, we would thus identify a plasmapause at L~10.2 during this pass.

In order to provide a more quantitative and reproducible criterion for identifying this transition, we consider the derived electron density and temperature. Figure 2b shows the density (blue) and temperature (red) for the same interval as shown in Figure 2a. As inferred from the spectrogram, the density in the inner magnetosphere (L<10) is fairly high (~2–3 cm^{-3}), and the temperature is low (< few tens of eV). There are a few brief intervals where the density drops and the temperature rises, an example of which is indicated by the red dashed arrow between the blue and red curves. These intervals are what have previously been identified as interchange injections. Beyond L~10, the peak density tends to decrease with increasing L, and the temperature is typically above ~100 eV, except for a few intervals where the density and temperature revert to values more characteristic of the inner magnetosphere (the blue dashed arrow shows an example). We interpret these colder, denser intervals as flux tubes carrying inner magnetospheric material outward as a consequence of interchange.

In the region between L~9 and 12 in Figure 2b, there is a considerable amount of high-frequency variation between dense/cool and tenuous/hot conditions. Much of this variation is attributable to the actuation of Anode 5, as described above. In Figure 3 this variability is removed by smoothing the density over 13

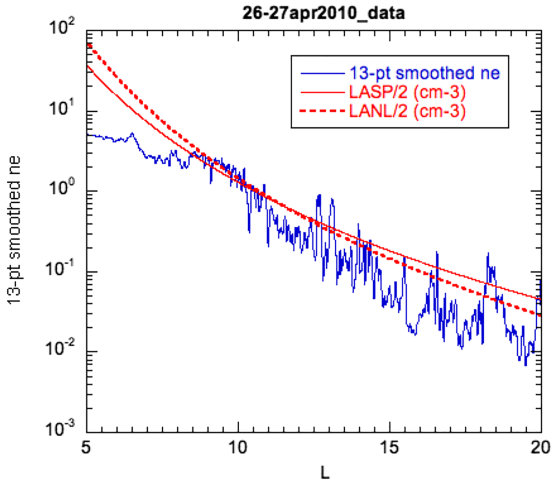

Figure 3. Thirteen-point smoothed electron density for the pass shown in Figure 2, plotted as a function of dipole L (blue curve). Also shown are the fits to the ion density measured on many orbits, calculated by Thomsen et al. (2010, dashed red curve) and Wilson et al. (2017, solid red curve). The ion density curves plotted here are one half of the actual fits reported by those two papers.

measurement points (roughly a full actuation period). The resulting smoothed density values are then plotted as a function of L, revealing rather clearly the two-state nature of the electron density beyond L~10. In Figure 3, fits to the equatorial ion densities obtained from the CAPS Ion Mass Spectrometer measurements are superimposed on the density plot for 26–27 April 2010. The red dashed line was derived by Thomsen et al. (2010) using the LANL numerical moments, and the red solid line was derived by Wilson et al. (2017) using the LASP forward modeling results. As given by Wilson et al., the two curves were

$$n_{\mathrm{LANL}}\ (\mathrm{cm}^{-3}) = 1.38{\times}10^{6}\ \mathrm{L}^{-5.68}$$

$$n_{\mathrm{LASP}}\ (\mathrm{cm}^{-3}) = 1.79{\times}10^{5}\ \mathrm{L}^{-4.84}$$

In Figure 3 we have used one half these values to obtain a better match with the derived electron densities. This is reasonable because there is roughly a factor of 3 variability in the inner magnetospheric density from pass to pass (Thomsen et al., 2010; Wilson et al., 2017) and because there is some uncertainty in the intercalibration of the ELS and IMS densities (e.g., Thomsen et al., 2018, who showed that the derived ion densities in the magnetosheath were typically a factor of 1.5–3 times the derived electron densities).

Figure 3 shows that the density in the higher-density intervals tends to fall off somewhat more slowly with L than the LASP ($L^{-4.84}$) or LANL ($L^{-5.68}$) fitted curves. If we interpret these higher-density, cooler regions as flux tubes loaded with inner magnetospheric plasma that have been transported by interchange out into the outer magnetosphere, we would expect the density to fall roughly as L^{-4}, preserving flux tube content in a nearly-dipolar field if the density is uniform throughout the flux tube or is confined near the equator with a scale height that varies linearly with L (as found for Saturn by Thomsen et al., 2010). The steeper fall-off of the LANL ion densities is attributable to the fact that that survey included all measured densities, including the low densities that are characteristic of the outer magnetosphere. This is less a factor in the LASP densities, which were largely restricted to higher-density, lower-temperature populations because of the constraints of the forward-modeling technique. Thus, it seems reasonable that the density of flux tubes loaded with inner magnetospheric plasma might fall off somewhere between L^{-4} (uniformly filled dipole field) and $L^{-4.84}$ (LASP).

Figure 4a shows the radial profile for the first eight passes through Saturn's inner/middle magnetosphere in 2010, a year in which the orbit remained near the equator, with inbound portions occurring near midnight local time and outbound portions near noon. In Figure 4a the inbound profiles are shown in light blue, and the outbound profiles in dark blue. The density scale on the y-axis is correct for the earliest pass (25–28 January), and every subsequent pass is offset by two orders of magnitude from the previous one. The red line in each pass corresponds to one half the LASP average ion density profile of Wilson et al. (2017). Figure 4a illustrates that the overall electron density profiles generally follow the average profile reasonably well from pass to pass, but there are substantial variations within individual passes, the expected signature of the interchange/reconnection processes described in the introduction. The density at L=10 generally lies within a factor of 2 or so of the Wilson curve (x1/2), reflecting the relatively steady inner magnetospheric population (see also Figure 2 of Wilson et al.). At L<8, the computed electron densities commonly fall below the ion density curve because the electron analysis does not account for negative spacecraft potentials, which frequently occur in the very dense and cold inner magnetosphere.

For the purposes of this study, the objective is to find a criterion that will reproducibly distinguish between the cold, dense plasma and the hot, tenuous plasma in the middle-outer magnetosphere. The “plasmapause” can then be identified as the distance at which the plasma transitions from mostly one type to mostly the other. Figure 4a suggests that the Wilson density curve, scaled to 1–2 cm^{-3} at L=10 would do a reasonably good job of separating dense from tenuous. On the other hand, it appears than in many cases the density of the “dense” intervals falls off somewhat less steeply than $L^{-4.84}$, closer to the L^{-4} estimated for conservation

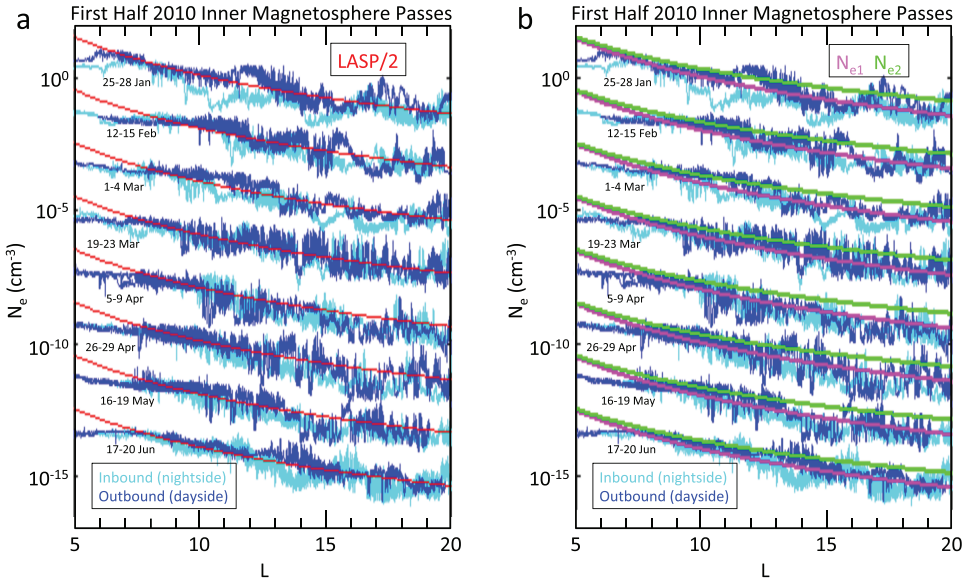

Figure 4. (a) Radial profile of electron density for the first eight passes through Saturn's inner/middle magnetosphere in 2010, with inbound portions (light blue) occurring near midnight local time and outbound portions (dark blue) near noon. Each pass subsequent to the first one is offset by two orders of magnitude from the previous one. The red line in each pass corresponds to one half the LASP average ion density profile of Wilson et al. (2017). (b) Same as a, but the magenta and green lines are the two adopted density curves for the dense/tenuous transition given in equations (1) and (2), respectively.

of flux-tube content. Hence, we define a range of density threshold curves that account for the observed pass-to-pass variability and uncertainties in the radial fall-off rate. The adopted curves are illustrated in Figure 4b as the magenta and green lines, corresponding to the following equations:

$$N_{e,1}\left(cm^{-3}\right) = 1.0\times(L/10)^{-4.84}\ (\text{magenta}) \tag{1}$$

$$N_{e,2}\left(cm^{-3}\right) = 2.0\times(L/10)^{-4}\ (\text{green}) \tag{2}$$

The observed electron density profiles tend not to follow the Wilson curve inside of L~8–10, partly because of the spacecraft potential issue mentioned above. Hence, the adopted thresholds for the inner magnetosphere (L<10) are simply set to the L=10 value of each curve (1.0 for threshold 1 and 2.0 for threshold 2). The following analysis is then conducted using both curves, and the results compared below. As a practical matter, the analysis is restricted to low magnetic latitudes (within ~5° of the equator). This is because the plasma density falls off significantly with latitude (e.g., Thomsen et al., 2010), and at high latitudes it is difficult to distinguish injections with low density and high temperatures from the low-density, outer plasma sheet/lobe environment. Since we are primarily interested in the region inside of L=20, where the current sheet warping is modest (Arridge et al., 2008), we have simply used an untilted dipole magnetic field for estimating the latitude.

With the threshold density conditions (1) and (2) (but flat inside L=10), the entire low-latitude dataset of CAPS electron moments is examined on a pass-by-pass basis. For each half-orbit (inbound or outbound), the measured densities are compared with the corresponding threshold values (equations (1) and (2), with the flat values below L=10). For each 0.1-Rs L-bin, the number of density values that are above/below the threshold are counted, and the fraction of dense values is recorded. Finally, the plasmapause is identified for each half-orbit as the L-value at which the fraction of high-density values falls below a specified level.

3. Results

Figure 5 shows examples of the results of the calculation of the fraction of dense values for two half-orbits in 2010. Figure 5a shows data from the outbound pass on 7–9 April 2010, and Figure 5b shows data from the

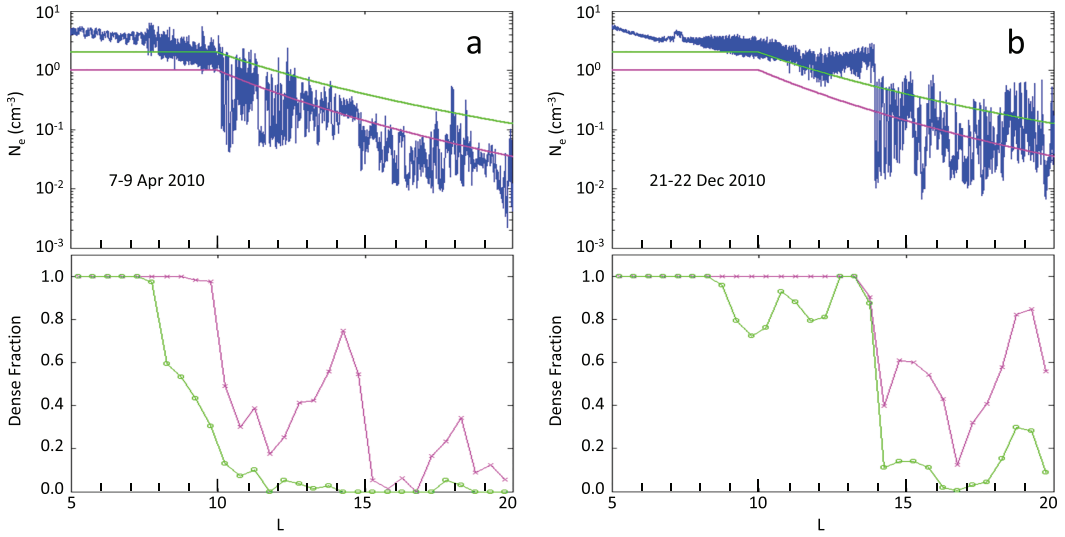

Figure 5. Radial profile of electron density and fraction of measurements with density above thresholds (magenta for equation (1); green for equation (2)) for (a) the outbound pass on 7–9 April 2010 and (b) the outbound pass on 21–22 December 2010.

outbound pass on 21–22 December 2010. The upper panel in each figure presents the electron density as a function of L, with the magenta and green curves showing the two adopted threshold densities from equations (1) and (2). The lower panels show the corresponding fraction of density values above threshold for each 0.5-Rs L-bin, with the same color coding. In both cases, there is a fairly clear transition from the mostly-dense inner magnetosphere to the mostly-tenuous outer magnetosphere, but Figure 1a shows that the location of this transition is dependent on the adopted threshold and can be as much as 2 Rs different for the range of adopted thresholds. Comparison of Figures 5a and 5b shows that the transition can also vary substantially for different passes.

Figures 6a and 6c summarize the results of this analysis for the entire low-latitude CAPS/ELS dataset, and Figures 6b and 6d show an expansion of the results for 2010, during which the spacecraft trajectory was nearly equatorial. Figures 6a and 6b show the results when density threshold 1 (equation (1)) was used to identify "dense" plasma, and Figures 6c and 6d show the results for threshold 2 (equation (2)). The grey areas in the plots indicate data gaps and intervals when the spacecraft was more than 5° away from the equator. The dense fraction in Figure 6 is plotted as a function of half-orbit number, and the Table S1 in the supporting information provides the mapping from half-orbit number to dates.

It is clear from the panels in Figure 6 that there is generally a transition from dominantly-dense conditions in the inner magnetosphere to dominantly-tenuous in the outer magnetosphere, with frequent intervals of non-dominant density conditions in both regions. The exact transition location depends on both the high/low density threshold used (equation (1) or (2)) and the fraction of dense measurements that is taken to denote the transition. Based on Figures 5a and 5b and similar plots for other passes, a value of 0.5 for the transition fraction is intuitively reasonable. We have also explored using transition fractions of 0.4 and 0.6 and find very little difference in the results; hence 0.5 is adopted for the remainder of this discussion.

Figure 7 summarizes the half-orbit by half-orbit determinations of L_{tran}, which is taken to be the lowest L value in any given half-orbit at which the dense fraction falls below 0.5. To avoid false identifications from brief intervals of data and/or passes where the dense inner magnetosphere is not seen (c.f., Figure 6), a value of L_{tran} is only determined if there exist at least 4 dense bins (where the fraction of densities above threshold is greater than 0.5) at L values below L_{tran}. The color-coding for the L_{tran} values is the same as used in earlier figures: magenta for density threshold 1 (equation (1)) and green for threshold 2 (equation (2)). The derived values of L_{tran} shown in Figure 7 mostly lie between L=8 and L=15, and as noted above, the higher threshold density (equation (2), green) results in generally lower values of L_{tran}.

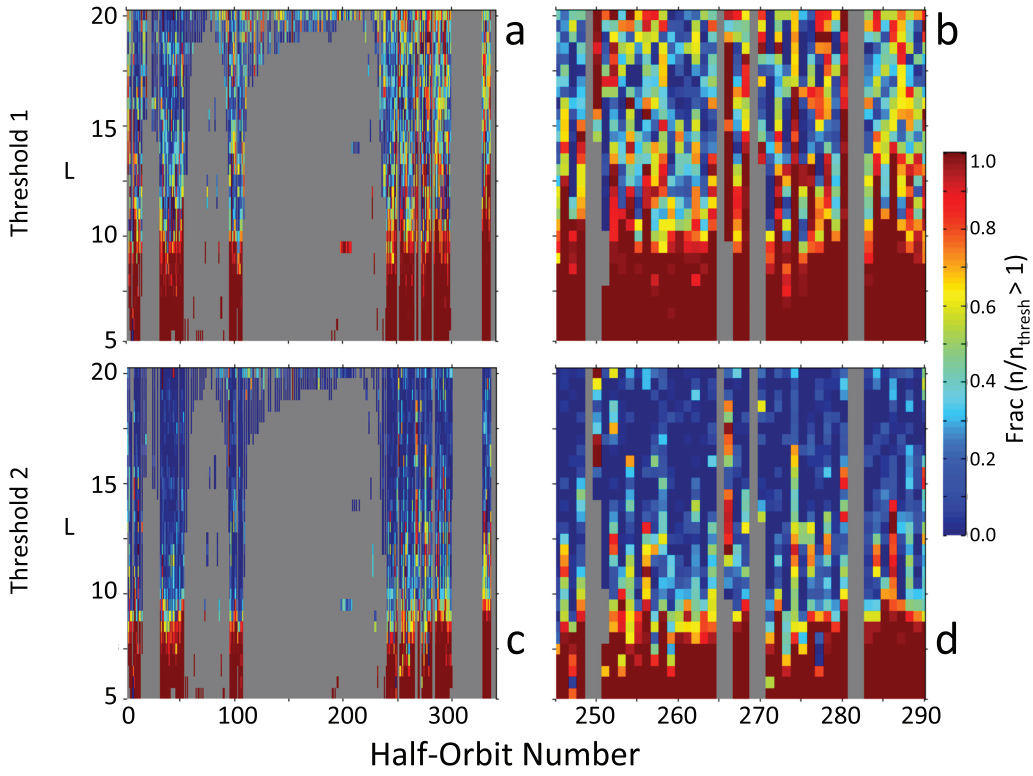

Figure 6. Fraction of measurements within each 0.5-Rs radial bin in each half-orbit that are above the density threshold: (a and b) Threshold 1 (equation (1)); (c and d) Threshold 2 (equation (2)). Panels a and c show the results for all low-latitude orbits, and panels b and d show only the orbits during 2010.

Figure 8a shows the distribution of L_{tran} values for the two different thresholds. The peak occurrence location is about 1 Rs larger for threshold 1 than for threshold 2. The peak occurrence for threshold 1 lies between ~9 and 11 Rs, whereas that for threshold 2 lies between ~8 and 10 Rs.

The data in Figures 6, 7, and 8a are given for the full range of local time in the dataset. In Figure 8b, the LT dependence of the L_{tran} distribution is examined. There is a very clear separation (~3 Rs) between the peak L_{tran} occurrence on the night-side (21–03 LT, blue solid circles) and the occurrence on the dayside (09–15 LT, red triangles). At dawn and dusk the statistics are poorer because of the sparser orbital coverage there, but the dawn peak (03–09 LT, magenta open circles) lies at a value of L_{tran} that is intermediate between the night-side and the dayside peaks. The dusk distribution (15–21 LT, green squares) is much broader and covers a range that encompasses both dayside and night-side peaks. The red bars in Figure 8c show the median value of L_{tran} for each 3-hr LT bin, confirming the day/night trend seen in the 6-hr bins plotted in Figure 8b. The open blue circles in Figure 8c indicate the number of half-orbits that contributed to each LT bin.

4. Discussion

This study has explored the paradigm that Saturn's plasmapause marks the boundary between the flux tubes that have been circulating around the planet for some time, accumulating a dense load of Enceladus-sourced material, and those that have recently undergone tail reconnection, shedding the bulk of the cold plasma and retaining a more tenuous, heated population. Since such a boundary should be unstable to the interchange instability, fingers of dense material should propagate out beyond the average plasmapause, while fingers of hot, tenuous material should propagate into the inner magnetosphere (i.e., interchange injections). In the middle magnetosphere of Saturn, a pattern of alternating dense, cool electrons and tenuous, hotter electrons is commonly observed, consistent with the expectations of this process. Thus, the position of the original boundary can be estimated by looking for the transition from mostly-dense-with-some-tenuous to mostly-tenuous-with-some-dense.

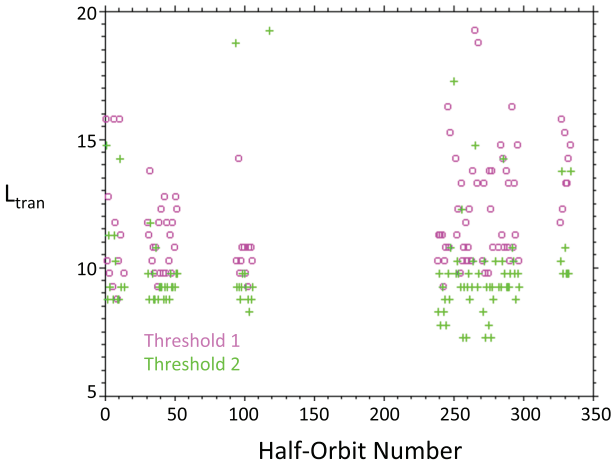

Figure 7. Lowest radial distance at which the fraction of density measurements above threshold falls below 0.5. Magenta points are based on density threshold 1 (equation (1)), and green points are based on density threshold 2 (equation (2)).

We have proposed a reproducible criterion for identifying this transition and have applied the criterion to previously computed CAPS/ELS electron moments. The results of course depend on the adopted threshold density for distinguishing "dense" from "tenuous". Guided by findings regarding the radial dependence of magnetospheric ion densities (e.g., Wilson et al., 2017), two functions for the threshold density have been identified as roughly bounding the "by-eye" transition for numerous individual half-orbits (equations (1) and (2), see Figure 4b). The higher threshold (equation (2)) gives lower transition distances than the lower threshold (Figure 7). We find (not shown) that where a transition distance is determined from both thresholds, 60% of the values of L_{tran} derived with equation (1) lie within 2 Rs of the corresponding values derived with equation (2), and 95% lie within 5 Rs.

Within this level of uncertainty, we find that most of the values of L_{tran} cluster in the neighborhood of L~10 (cf., Figure 8), but that there can be considerable variation from pass to pass, with some measured values exceeding L~15. The implication is that the boundary between tail-reconnected flux tubes and not-yet-reconnected inner magnetospheric flux tubes generally lies near L~10. This is in accord with our earlier

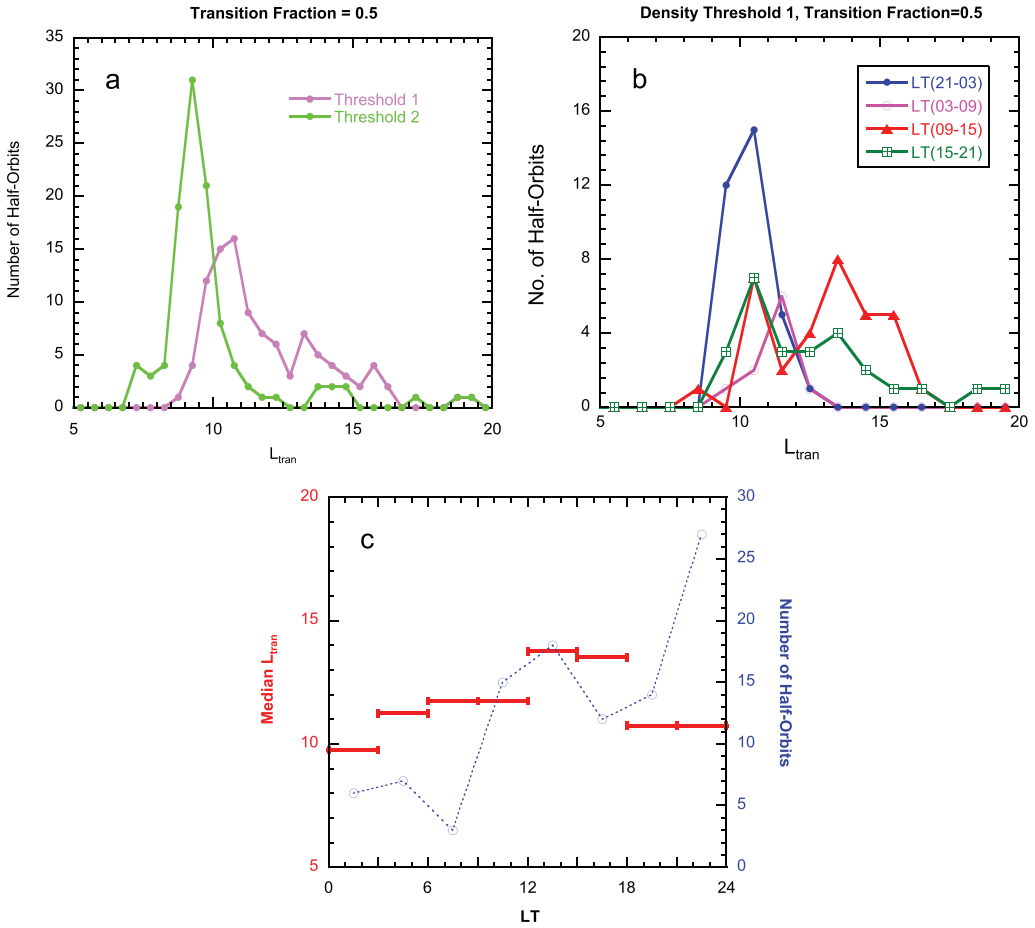

Figure 8. (a) Occurrence distribution of derived L_{tran} based on density threshold 1 (equation (1), magenta) and density threshold 2 (equation (2), green). (b) Occurrence distribution of L_{tran} based on density threshold 1 for four different local time sectors (21–03 blue filled circles, 03–09 magenta open circles, 09–15 red triangles, and 15–21 green squares). (c) Median value of L_{tran} based on density threshold 1 for 3-hr local time bins, plotted as a function of LT.

finding for a single event (Thomsen et al., 2015) that tail reconnection can strip off dense inner magnetospheric plasma into as deep as L~8.6.

This does not mean that the reconnection distance in the tail is only ~10 Rs, however: The prereconnection flux tubes will be greatly stretched tailward, and subsequent to reconnection they will contract sunward into a more dipolar configuration, in which we finally locate the plasmapause boundary. Rather, it suggests that the reconnection distance maps to an ionospheric latitude that corresponds to a dipole L~10, i.e., a latitude of ~72°. In the simplified model of a dipole plus magnetodisc examined by Achilleos et al. (2010), dipolar field lines that cross 10–12 Saturn radii at the equator are displaced to equatorial distances 16–25 Rs by the external currents. A more advanced version of this UCL/AGA model (Sorba et al., 2019) shows that the mapping from the ionosphere varies with local time: In the midnight region, an ionospheric latitude of 71.6° North maps to downtail distances of 16.5 and 31.4 Rs under "compressed" and "expanded" conditions of the model, respectively. Mapping from the same latitude in the southern hemisphere produces even larger equatorial crossing distances (36 and 54 Rs, respectively). On the other hand, the magnetic field models of Belenkaya et al. (2016) and Khurana et al. (2006) yield equatorial crossing distances of a field line originating at an invariant latitude of 71.6° that are very close to 10 Rs for a variety of conditions, with significant stretching not occurring until somewhat larger radial distances (and ionospheric latitudes). Observations of outward-propagating reconnection signatures (Smith et al., 2016) show evidence of a significant number of reconnection events occurring as close as 20 Rs to the planet. The plasmoid described by Hill et al. (2008) was inferred to have originated at ~20 Rs from the planet, and the ENA enhancement event attributed to current sheet collapse (tail reconnection) by Mitchell et al. (2005) originated at or beyond Titan's orbit (20 Rs). Thus, there is credible evidence that the plasmapause we identify may well map to a downtail reconnection distance of 20 Rs or more.

Because it is the steep inward gradient in the flux-tube content that drives the interchange instability, the results found here further suggest that the interchange (inward motion of hot, tenuous plasma and outward flow of cold, dense material) typically begins near L~10 as well, though with some variability. Phase-space density mapping for high-energy electrons in two injection events (Paranicas et al., 2016) suggested that those events originated at somewhat smaller values, ~7–9 Rs. As already noted, the event studied by Thomsen et al. (2015) showed outward-flowing cool, dense plasma fingers at L~8.6.

The results presented in Figure 8 indicate that there is a local time asymmetry to the typical plasmapause distance, namely that the post-noon plasmapause tends to be ~3–4 Rs further from the planet than the night-side location. In the paradigm described above, the location of the plasmapause is set by the distance to the night-side reconnection point (followed by subsequent dipolarization). Thereafter, the boundary should simply convect along the cold-plasma drift path onto the dayside. The day-night offset found in this study may be a reflection of the dawnward drift noted previously in the inner magnetosphere (Andriopoulou et al., 2012, 2014; Thomsen et al., 2012; Wilson et al., 2013). Indeed, the convection pattern inferred in those studies exhibits a rotation of the symmetry axis toward local times slightly later than midnight/noon (Andriopoulou et al., 2014; Wilson et al., 2013), similar to the plasmapause distance shown in Figure 8c.

5. Conclusions

Reconnection of stretched flux tubes loaded with inner magnetospheric cool plasma, with consequent loss downtail, is a plausible explanation of the dominance of warmer, more tenuous plasma in the middle-outer magnetosphere. The subsequent action of an interchange instability driven by the resulting radial gradient in the flux-tube content is a similarly plausible explanation for the presence of alternating regions of cool, dense electrons and hotter, more tenuous electrons in the middle magnetosphere. The denser population found there is typically connected to the dense inner magnetospheric density by an L^{-n} relationship, where n~4, consistent with conservation of flux tube content.

The distance at which the electron density transitions from mostly-dense-with-some-tenuous to mostly-tenuous-with-some-dense is identified as the plasmapause, the boundary between flux tubes that have undergone night-side reconnection and those that have not. Analysis of CAPS/ELS data suggests that this boundary typically occurs near and somewhat beyond L~10, with variation from pass to pass. Some models of the stretched night-side magnetic field indicate that an L=10 boundary could correspond to a downtail reconnection distance ~20 Rs or more. There is also a local time dependence such that the plasmapause is

typically seen at larger radial distances on the day side than on the night side. This offset may be related to the previously reported dawnward convection pattern observed in the inner magnetosphere.

Acknowledgments
The authors thank Arianna Sorba, Nick Achilleos, Elena Belenkaya, and Krishan Khurana for providing the mapping results of their magnetic field models. Work at PSI was supported by the NASA Cassini program through JPL contract 1243218 with Southwest Research Institute. The Cassini project is managed by the Jet Propulsion Laboratory for NASA. A. J. C. acknowledges support from STFC, UK, via the solar system consolidated grant to MSSL ST/S000240/1. The Cassini ELS moments used for this study are available from the Planetary Data System (http://pds.nasa.gov/). Cassini trajectory information was calculated from the CAPS/ANC files within the PDS data volume CO- E/J/S/SW-CAPS-2-UNCALIBRATED-V1.0.

References

Achilleos, N., Guio, P., & Arridge, C. S. (2010). A model of force balance in Saturn's magnetodisc. *Monthly Notices of the Royal Astronomical Society*, *401*, 2349–2371. https://doi.org/10.1111/j.1365-2966.2009.15865.x

Andriopoulou, M., Roussos, E., Krupp, N., Paranicas, C., Thomsen, M., Krimigis, S., et al. (2012). A noon-to-midnight electric field and nightside dynamics in Saturn's inner magnetosphere, using microsignature observations. *Icarus*, *220*, 503–513. https://doi.org/10.1016/j.icarus.2012.05.010

Andriopoulou, M., Roussos, E., Krupp, N., Paranicas, C., Thomsen, M., Krimigis, S., et al. (2014). Spatial and temporal dependence of the convective electric field in Saturn's inner magnetosphere. *Icarus*, *229*, 57–70. https://doi.org/10.1016/j.icarus.2013.10.028

Arridge, C. S., Khurana, K. K., Russell, C. T., Southwood, D. J., Achilleos, N., Dougherty, M. K., et al. (2008). Warping of Saturn's magnetospheric and magnetotail current sheets. *Journal of Geophysical Research*, *113*, A08217. https://doi.org/10.1029/2007JA012963

Belenkaya, E. S., Kalegaev, V. V., Cowley, S. W. H., Provan, G., Blokhina, M., Barinov, O. G., et al. (2016). Optimization of Saturn paraboloid magnetospheric field model parameters using Cassini equatorial magnetic field data. *Annales Geophysicae*, *34*, 641–656. https://doi.org/10.5194/angeo-34-641-2016

Coates, A. J., Alsop, C., Coker, A. J., Linder, D. R., Johnstone, A. J., Woodliffe, R. D., et al. (1996). The electron spectrometer for the Cassini spacecraft. *Journal of the British Interplanetary Society*, *45*(9).

Hill, T. W., Thomsen, M. F., Henderson, M. G., Tokar, R. L., Coates, A. J., McAndrews, H. J., et al. (2008). Plasmoids in Saturn's magnetotail. *Journal of Geophysical Research*, *113*, A01214. https://doi.org/10.1002/2015JA022005

Khurana K.K., Arridge, C.S., Schwarzl, H., and Dougherty, M.K. (2006). A model of Saturn's magnetospheric field based on latest Cassini observations, presented at the Spring AGU meeting, Baltimore.

Lai, H. R., Russell, C. T., Jia, Y. D., Wei, H. Y., & Dougherty, M. K. (2016). Transport of magnetic flux and mass in Saturn's inner magnetosphere. *Journal of Geophysical Research: Space Physics*, *121*, 3050–3057. https://doi.org/10.1002/2016JA022436

Lewis, G. R., Andre, N., Arridge, C. S., Coates, A. J., Gilbert, L. K., Linder, D. R., & Rymer, A. M. (2008). Derivation of density and temperature from the Cassini-Huygens CAPS electron spectrometer. *Planetary and Space Science*, *56*, 901–912. https://doi.org/10.1016/j.pss.2007.12.017

Linder, D. R., Coates, A. J., Woodliffe, R. D., Alsop, C., Johnstone, A. D., Grande, M., et al. (1998). The Cassini CAPS Electron Spectrometer. In *Measurement techniques in space plasmas: Particles*, geophysical monograph series, (Vol. *102*, pp. 257–262). Washington, D.C: American Geophysical Union.

Mitchell, D. G., Brandt, P. C., Roelof, E. C., Dandouras, J., Krimigis, S. M., Mauk, B. H., et al. (2005). Energetic ion acceleration in Saturn's magnetotail: Substorms at Saturn? *Geophysical Research Letters*, *32*, L20S01. https://doi.org/10.1029/2005GL022647

Paranicas, C., Thomsen, M. F., Achilleos, N., Andriopoulou, M., Badman, S. V., Hospodarsky, G., et al. (2016). Effects of radial motion on interchange injections at Saturn. *Icarus*, *264*, 342–351. https://doi.org/10.1016/j.icarus.2015.10.002

Smith, A. W., Jackman, C. M., & Thomsen, M. F. (2016). Magnetic reconnection in Saturn's magnetotail: A comprehensive magnetic field survey. *Journal of Geophysical Research: Space Physics*, *121*, 2984–3005. https://doi.org/10.1002/2015JA022005

Sorba, A. M., Achilleos, N. A., Sergis, N., Guio, P., Arridge, C. S., & Dougherty, M. K. (2019). Local time variation in the large-scale structure of Saturn's magnetosphere. *Journal of Geophysical Research: Space Physics*, *124*, 7425–7441. https://doi.org/10.1029/2018JA026363

Southwood, D. J., & Kivelson, M. G. (1987). Magnetospheric interchange instability. *Journal of Geophysical Research*, *92*, 109–116. https://doi.org/10.1029/JA092iA01p00109

Thomsen, M. F. (2013). Saturn's magnetospheric dynamics. *Geophysical Research Letters*, *40*, 5337–5344. https://doi.org/10.1002/2013GL057967

Thomsen, M. F., Coates, A. J., Jackman, C. M., Sergis, N., Jia, X., & Hansen, K. C. (2018). Survey of magnetosheath plasma properties at Saturn and inference of upstream flow conditions. *Journal of Geophysical Research: Space Physics*, *123*, 2034–2053. https://doi.org/10.1002/2018JA025214

Thomsen, M. F., Mitchell, D. G., Jia, X., Jackman, C. M., Hospodarsky, G., & Coates, A. J. (2015). Plasmapause formation at Saturn. *Journal of Geophysical Research: Space Physics*, *120*, 2571–2583. https://doi.org/10.1002/2015JA021008

Thomsen, M. F., Reisenfeld, D. B., Delapp, D. M., Tokar, R. L., Young, D. T., Crary, F. J., et al. (2010). Survey of ion plasma parameters in Saturn's magnetosphere. *Journal of Geophysical Research*, *115*, A10220. https://doi.org/10.1029/2010JA015267

Thomsen, M. F., Roussos, E., Andriopoulou, M., Kollmann, P., Arridge, C. S., Paranicas, C. P., et al. (2012). Saturn's inner magnetospheric convection pattern: Further evidence. *Journal of Geophysical Research*, *117*, A09208. https://doi.org/10.1029/2011JA017482

Wilson, R. J., Bagenal, F., Delamere, P. A., Desroche, M., Fleshman, B. L., & Dols, V. (2013). Evidence from radial velocity measurements of a global electric field in Saturn's inner magnetosphere. *Journal of Geophysical Research: Space Physics*, *118*, 1–11. https://doi.org/10.1002/jgra.50251

Wilson, R. J., Bagenal, F., & Persoon, A. M. (2017). Survey of thermal plasma ions in Saturn's magnetosphere utilizing a forward model. *Journal of Geophysical Research: Space Physics*, *122*, 7256–7278. https://doi.org/10.1002/2017JA024117

Young, D. T., Berthelier, J. J., Blanc, M., Burch, J. L., Coates, A. J., Goldstein, R., et al. (2004). Cassini plasma spectrometer investigation. *Space Science Reviews*, *114*(1-4), 1–112. https://doi.org/10.1007/s11214-004-1406-4

Young, D. T., Berthelier, J.-J., Blanc, M., Burch, J. L., Coates, A. J., Goldstein, R., et al. (2005). Composition and dynamics of plasma in Saturn's magnetosphere. *Science*, *307*, 1262–1266.